Stability of highly asymmetric non-neutral plasmas

E. Yu. Backhaus, J. Fajans, and J. S. Wurtele
Department of Physics, University of California–Berkeley, Berkeley, California 94720-7300

(Received 24 March 1998; accepted 10 September 1998)

The stability of non-neutral plasma equilibria subjected to external, azimuthal–asymmetric potentials is studied. The system exhibits a wide range of complex, symmetry-dependent, bifurcation phenomena. © *1999 American Institute of Physics.* [S1070-664X(99)01601-8]

I. INTRODUCTION

When non-neutral plasma columns are subject to azimuthally asymmetric electrostatic potentials, they deform into azimuthally asymmetric shapes.[1–3] A typical asymmetric shape is shown in Fig. 1. The companion paper[4] presents methods of predicting the form of these shapes. Here we analyze the shapes' stability. Stability is normally studied through modal analysis, in which nonlinear equilibria are calculated and subsequently perturbed. Eigenvalue collisions are often assumed to engender instability. However, as is well known in bifurcation theory,[5–7] symmetries can stabilize eigenvalue collisions. We have two goals in this paper: (1) to describe the various, often surprising, responses that the plasma makes to the applied perturbations, and (2) to illustrate, in a realizable physical system, some of the complicated Hamiltonian bifurcation phenomenon that occur in systems which possess a high degree of symmetry.

The non-neutral plasma columns are confined in Penning–Malmberg traps.[8] A schematic of the system is shown in the companion paper.[4] The plasma is held within a conducting cylindrical wall of radius R. Radial confinement is provided by a uniform axial magnetic field ($\mathbf{B}=B\hat{\mathbf{z}}$), while axial confinement is provided by an electrostatic well. More detailed descriptions of Penning–Malmberg traps can be found in the literature.[9,10]

We make the common assumption that the axially ($\hat{\mathbf{z}}$)-directed motion bounce averages out, and that the system can be described by the two-dimensional (2D) drift Poisson equations. Then only motion in the (r,θ) plane perpendicular to $\mathbf{B}$ is important, and the particles follow $\mathbf{E}\times\mathbf{B}$ orbits, where the $\mathbf{E}$ field is determined by both the plasma itself and the imposed boundary condition at the cylindrical wall, $V=V(\theta)$. The 2D drift Poisson equations are isomorphic to the 2D Euler equations for incompressible, inviscid fluids.[11] In this isomorphism, the plasma charge density corresponds to the fluid vorticity and the electrostatic potential corresponds to the stream function. Thus results obtained for non-neutral plasmas are also applicable to 2D fluid flows.

In the case of a grounded confining wall $[V(\theta)=0]$, the steady-state solution of the equations of motion is a centered, circular plasma.[12] Breaking the symmetry $[V(\theta)\neq 0]$ deforms the plasma. While Chu *et al.*[13] used perturbation techniques to prove that the plasma remains stable under small external potentials $V(\theta)$, it seems intuitively plausible that sufficiently large potentials should lead to instability. However, some experimentally stable plasmas are so distorted that they cannot be described by perturbation theory. Understanding the stability properties of these highly deformed plasmas was the original motivation for this work.

Contour dynamics-based[14,15] numerical studies of asymmetric plasmas reveal complicated dynamical behaviors that cannot be interpreted easily. In an attempt to clarify the picture of the transition to instability, we employ a framework developed for the study of bifurcations in Hamiltonian systems.[16] Two types of bifurcations occur in our system: steady-state and Krein–Hopf collisions. We use recently proven theorems[5,7] on the generic behavior of Hamiltonian systems with a single bifurcation parameter to make general predictions for the behavior of our system. These predictions strongly depend on the system symmetries. We numerically investigate several systems with different symmetries, and compare the results with our predictions. As no disagreements are observed, we conclude that the symmetry arguments can be employed profitably.

The influence of symmetry on stability has been studied theoretically in both dissipative and Hamiltonian systems. While many practical dissipative systems (Taylor–Couette flow, Rayleigh–Benard convection to name a few) can be found in the literature, few practical Hamiltonian systems have been discussed. Asymmetric plasma equilibria are a good practical example of a complicated Hamiltonian system with symmetries determined by the boundary condition. The flexibility of the boundary condition makes these systems particularly interesting.

We begin, in Sec. II, by studying elliptical equilibria, for which there exists a simple analytical treatment that allows us to probe the stability problem. In Sec. III, the method of contour dynamics, here slightly modified, is presented briefly, and the linear stability analysis is developed. Section IV studies the stability of symmetric systems. The change of the eigenvalue spectrum is investigated numerically as the strength of the external potential is varied. Crossings with other equilibrium branches are studied. Comparisons show a clear agreement between predictions based on the bifurcation theory for Hamiltonian systems and numerical results for the steady-state bifurcations. We show the scaling of the instability threshold with the plasma area. Stability in a system with no rotational symmetries is investigated in Sec. V, using the example of a circular off-center equilibrium. Appendix A gives a detailed derivation of the contour dynamics equa-

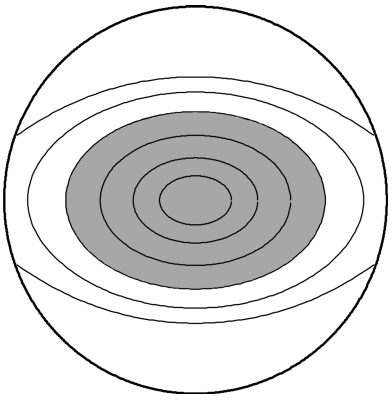

FIG. 1. Elliptical on-center plasma equilibrium. The plasma covers the shaded region. The light solid lines are equipotential contours, and the heavy surrounding circle is the trap's cylindrical boundary.

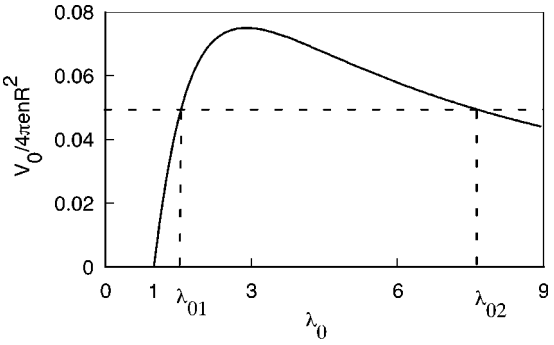

FIG. 2. Equilibrium ellipticity λ_0 vs the external potential V_0, from Eq. (5).

tions, and Appendix B gives a proof, based on energetics, that circular, off-axis plasmas are stable.

II. ELLIPTICAL EQUILIBRIA

Elliptical plasmas can be described by a simple analytical treatment—the elliptical plasma model developed by Chu *et al.*[13] In this model, which is valid for plasmas of small area, extended patches of charge are assumed to have elliptical shapes. Chu *et al.* approximate the exact particle guiding-center Hamiltonian by including only a finite number of degrees of freedom, namely the center of charge with coordinates (x_c, y_c), the aspect ratio λ, and the angle between major axis and x-axis φ. We use a boundary potential $V=-V_0\cos 2\theta$, which we expect to result in an elliptical equilibrium for small plasmas. Without loss of generality the bifurcation parameter V_0 is taken to be positive.

To lowest order in the plasma area A_p, the system is described by the equations of motion:[13]

$$\dot{x}_c=-\frac{2c}{B}\left(\frac{V_0}{R^2}+\frac{enA_p}{R^2-x_c^2-y_c^2}\right)y_c, \tag{1}$$

$$\dot{y}_c=-\frac{2c}{B}\left(\frac{V_0}{R^2}-\frac{enA_p}{R^2-x_c^2-y_c^2}\right)x_c, \tag{2}$$

$$\dot{\lambda}=-\frac{4enc}{B}\frac{A_p\lambda}{(R^2-x_c^2-y_c^2)^2}[2x_cy_c\cos 2\varphi - (x_c^2-y_c^2)\sin 2\varphi]-\frac{4c\lambda V_0}{BR^2}\sin 2\varphi, \tag{3}$$

$$\dot{\varphi}=\frac{4\pi cen\lambda}{B(\lambda+1)^2}+\frac{2cen}{B}\frac{\lambda^2+1}{\lambda^2-1}\left(\frac{A_p}{(R^2-x_c^2-y_c^2)^2}\times[(x_c^2-y_c^2)\cos 2\varphi+2x_cy_c\sin 2\varphi]-\frac{V_0}{enR^2}\cos 2\varphi\right). \tag{4}$$

The system governed by Eqs. (1)–(4) is Hamiltonian and the explicit expression for the Hamiltonian can be found in Ref. 13. Note that the equations of motion possess $\mathbf{Z_2}\times\mathbf{Z_2}$ symmetry with reflections $(x_c,y_c,\lambda,\varphi)\rightarrow(-x_c,-y_c,\lambda,\varphi)$ and $(x_c,y_c,\lambda,\varphi)\rightarrow(x_c,y_c,\lambda,\varphi+\pi)$. The first reflection corresponds to the reflection of the center of charge and the second to the rotation of the ellipse by π. From Eqs. (1) and (2) it is clear that a centered plasma $[(x_c,y_c)=(0,0)]$ is a likely equilibrium. Solving Eqs. (3) and (4) for $\dot{\lambda}=0$ and $\dot{\phi}=0$ with $(x_c,y_c)=(0,0)$ we obtain an equilibrium for $\phi=0,\pi$ and $\lambda=\lambda_0$, where λ_0 satisfies the equation

$$\frac{V_0}{2\pi enR^2}=\frac{\lambda_0(\lambda_0^2-1)}{(1+\lambda_0)^2(1+\lambda_0^2)}. \tag{5}$$

As expected, the strength of the external potential determines the ellipticity of the equilibrium. The plot of the right-hand side of Eq. (5), presented in Fig. 2, shows that there are two solutions of Eq. (5) $(\lambda_{01},\lambda_{02};\lambda_{01}<\lambda_{02})$ for $V_0/4\pi enR^2\leqslant 0.07507$ and no solution for $V_0/4\pi enR^2>0.07507$. Thus there are two (up to the π rotation of the ellipse) on-center solutions with different ellipticity.

To determine the stability of these equilibria, we linearize the equations of motion. The equations for the position of the center of charge and the ellipticity separate. The Jacobian of the linearized form for the center of charge is

$$J_{xy}=-\frac{4c^2}{B^2R^4}(V_0-enA_p)(V_0+enA_p). \tag{6}$$

Thus the instability threshold for the on-center equilibrium is

$$V_0^{\text{th}}=enA_p, \tag{7}$$

because for $V_0\leqslant V_0^{\text{th}}$ the Jacobian J_{xy} is positive and the resulting eigenvalues are pure imaginary, yielding stable motion of the center of charge. Note that the trap radius R does not appear in threshold criterion, as both the applied and image fields vary as $1/R^2$ for a small plasma close to the origin.

The cause of instability in this system is apparent from the center of charge equations of motion [Eqs. (1) and (2)]. In the small plasma approximation, the motion of the center of charge is along the equipotential line of the combined image and external potentials. If the equilibrium is displaced from the origin, the image charge attempts to induce a stable rotation around the origin. The external potential, however,

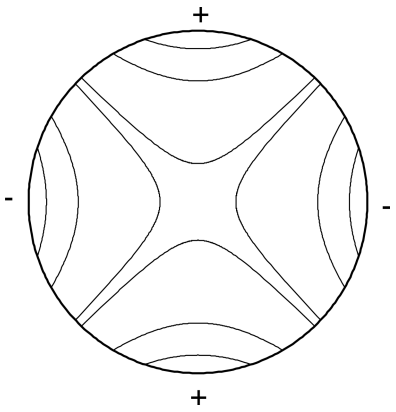

FIG. 3. Potential contours for elliptical external potential.

tends to move the center of charge away from the origin, as can be seen in the equipotential plot, Fig. 3. Thus the external potential attempts to destabilize the equilibrium. Instability results if the external electric field is larger than the image charge field. In the language of non-neutral plasmas, the diocotron frequency[12,17] goes to zero and the diocotron motion stalls, and then destabilizes.

The ellipticity equation [Eq. (3)] must be analyzed to complete the stability evaluation. After calculating the Jacobian, one can see that the equilibrium with λ_{01} is stable, while the one with λ_{02} is unstable. The value of the parameter $V_0/4\pi enR^2=0.07507$ corresponds to the saddle–node bifurcation where the stable and unstable branches coalesce.

Combining the stability analysis for the center of charge and ellipticity, we conclude that the on-center equilibrium with ellipticity given by λ_{01} is stable for $0\leqslant|V_0|\leqslant enA_p$. At the instability threshold the Jacobian $J_{xy}=0$, and intersections with other equilibrium branches are possible. To investigate this possibility, a bifurcation analysis close to the threshold could be performed or, alternatively, other equilibria may be found by inspection from equations of motion. Following the latter path we find from Eqs. (1) and (2) that another equilibrium exists for $V_0>enA_p$, with

$$x_c=\pm R\sqrt{1-\frac{enA_p}{V_0}},\quad y_c=0. \tag{8}$$

Equations (3) and (4) yield the equilibrium values of ϕ and λ. Stability analysis reveals that this equilibrium is stable. Thus, at the instability threshold, given by Eq. (7), the on-center equilibrium experiences a supercritical pitchfork bifurcation. A new branch of solutions appears which corresponds to the off-center equilibrium Eq. (8). An exchange of stability occurs. Note that this new equilibrium, as is typical in bifurcation theory, is not symmetric with respect to the reflection of the center of charge.

In summary, the elliptical plasma model provides some insight into the stability problem. The transition to instability of the on-center static shape is observed. Crossing with other equilibrium branches occurs. Further investigations of other equilibria corresponding to different boundary conditions are needed to generalize the results to arbitrary wall potentials. Unfortunately, the elliptical plasma model is not suitable for investigating the equilibria and stability for arbitrary wall potentials as moments beyond the first and second (i.e., center of charge and ellipticity) become important in the dynamics. A technique that allows us to find equilibria and analyze stability in the general case is developed in the next section.

III. CONTOUR DYNAMICS AND STABILITY ANALYSIS

Consider the full equations of motion for a long, magnetized electron column: the continuity equation for the electron density (n), the $\mathbf{E}\times\mathbf{B}$ drift equation, and Poisson's equation for the electrostatic potential satisfying the boundary condition $\phi(R,\theta)=V(\theta)$. When, as is common, the plasma temperature is so low that the Debye length λ_D is small compared to the plasma radius, the electron density becomes nearly constant in the plasma interior and decays to zero on the scale of λ_D (Ref. 18) at the plasma edge. Therefore we will use the flat top, constant density plasma model. More realistic, smooth density equilibria will be considered in Sec. VI. To simplify the problem further only plasma shapes consisting of a single simply connected region of nonzero density are considered.

In Sec. IV symmetries of the system will be used to predict instability. The equations of motion themselves have SO(2) symmetry, and the symmetry of the problem is determined by the boundary condition, i.e., by the wall potential $V(\theta)$. For example, a system with a constant applied potential has SO(2) symmetry. The family of external potentials given by $V(\theta)=-V_0\cos m\theta$, which will be considered in Sec. IV, results in $\mathbf{Z_m}(2\pi/m)$ symmetry (the symmetry generated by rotations in θ of $2\pi/m$).

In-flows with constant charge density, the velocity at any point in space depends solely on the location of the plasma boundary. The methodology of contour dynamics[14,19] (CD), first developed for fluid dynamics, uses this simplification. Here we must modify the standard CD formalism to include the boundary condition at the confining wall.[15] We use CD throughout this paper to obtain static shapes numerically, to investigate stability, and to perform dynamic simulations.

The electrostatic potential for the system at hand can be represented as

$$\phi=\phi_p+\phi_i+\phi_{\rm ext}, \tag{9}$$

where ϕ_p corresponds to the free space plasma potential, ϕ_i is the image contribution, and $\phi_{\rm ext}$ is the external potential. For flat top plasmas, the expression for the free space potential written using the Green's function combined with the Stoke's theorem yields[14]

$$\phi_p(x,y)=ne\left(-A_p+\oint_C \ln|\mathbf{r}-\mathbf{r}'|\times[(x'-x)dy'-(y'-y)dx']\right), \tag{10}$$

where A_p is the plasma area and integration is performed over the plasma boundary C. We express the image and external contributions inside the cylindrical domain as solutions of Laplace's equation in cylindrical coordinates subject to the boundary conditions $\phi_i(R,\theta)=-\phi_p(R,\theta)$ and

$\phi_{\rm ext}(R,\theta)=V(\theta)$. We calculate the velocity of the flow from the electrostatic potential as $\mathbf{v}=-c\nabla\phi\times\hat{\mathbf{z}}/B$, giving

$$\mathbf{v}(x,y)=-\frac{2enc}{B}\oint_C \ln|\mathbf{r}-\mathbf{r}'|d\mathbf{x}'-c\frac{\nabla(\phi_i+\phi_{\rm ext})\times\hat{\mathbf{z}}}{B}. \tag{11}$$

Turning to the static problem of equilibrium plasma shapes, recall that in $\mathbf{E}\times\mathbf{B}$ dynamics, the guiding centers of the plasma electrons drift along the equipotential contours. Therefore, for flat top plasmas the shape is stationary if the electrostatic potential on the plasma boundary $r_p(\theta)$ is equal to a constant,[13] i.e.,

$$\phi(r_p(\theta),\theta)=\text{const.} \tag{12}$$

Writing the CD expression for the potential on the plasma boundary, a static shape can be found using Eq. (12). Details of the numerical calculation can be found in Refs. 15 and 20. What about the stability of asymmetric equilibria subject to possible $\mathbf{E}\times\mathbf{B}$ perturbations? Though general nonlinear stability conditions would be preferable, we consider weaker spectral stability conditions due to the complicated nature of the problem. Our analysis is similar to that in Ref. 21, where stability of different vortex configurations was investigated, extended here to include the external and image potentials.

Two cylindrical coordinate systems will be used frequently in this paper: (r,θ) centered on the trap, and (ξ,η) centered inside the plasma at x_c,y_c. The plasma boundary in the second system is

$$x_p(\theta)=x_c+\xi(\eta)\cos\ \eta,\quad y_p(\theta)=y_c+\xi(\eta)\sin\ \eta. \tag{13}$$

Let $\xi_0(\eta)$ be the equilibrium state of the system. Then the perturbed state can be represented as

$$\xi(\eta)=\xi_0(\eta)+\delta\xi(\eta), \tag{14}$$

where $\delta\xi(\eta)$ is assumed to be small. The perturbation, $\delta\xi(\eta)=\tilde{\xi}(\eta)e^{\sigma t}$ is assumed to be a normal mode of the system. Velocities are represented as

$$\mathbf{v}(\eta)=\mathbf{v}_0(\eta)+\tilde{\mathbf{v}}(\eta)e^{\sigma t}. \tag{15}$$

The flow velocity determines the evolution of the boundary:

$$\frac{D\xi}{Dt}=\frac{\partial\xi}{\partial t}+\frac{v_\eta}{\xi}\frac{\partial\xi}{\partial\eta}=v_\xi. \tag{16}$$

Linearizing this equation of motion using Eqs. (14) and (15) yields

$$\sigma\tilde{\xi}+\frac{v_{\eta_0}}{\xi_0}\frac{d\tilde{\xi}}{d\eta}+\frac{\tilde{v}_\eta}{\xi_0}\frac{d\xi_0}{d\eta}-\frac{v_{\eta_0}}{\xi_0^2}\frac{d\xi_0}{d\eta}\tilde{\xi}=\tilde{v}_\xi. \tag{17}$$

We express the velocity amplitude as a linear functional of the boundary shape ξ, using the contour dynamics equation [Eq. (11)], and substitute it into Eq. (17). The normal mode amplitude function $\tilde{\xi}(\eta)$ is represented in the form

$$\tilde{\xi}(\eta)=\xi_0(\eta)\sum_{l=1}^{\infty}C_l f_l(\eta), \tag{18}$$

where $\{f_l\}$ stands for a set of orthonormal functions and the expansion is multiplied by the basic state ξ_0 for convenience. Due to the periodicity of the system in η a natural choice for the basis $\{f_l\}$ is

$$\{f_l\}=\frac{1}{\sqrt{\pi}}\left\{\frac{1}{\sqrt{2}},\cos\ \eta,\cos 2\eta\ldots,\sin\ \eta,\sin 2\eta\ldots\right\}. \tag{19}$$

Using Galerkin's projection method, we keep only a finite number N_l of basis functions. Taking the inner product of Eq. (17) with f_l yields an eigenvalue problem

$$\sigma C_m=\sum_{l=1}^{N_l}G_{ml}C_l. \tag{20}$$

Explicit expression for the $N_l\times N_l$ matrix G_{ml} can be found in Appendix A. The stability of the equilibrium can now be deduced from the spectrum of G. If all the eigenvalues σ_j have nonpositive real parts, the system is stable; otherwise, it is unstable. We can compute numerically the eigenvalues and eigenvectors for any equilibrium shape of interest.

When no external potential is present, the equilibrium is a circle of arbitrary radius r_p, and the perturbed states are the much studied diocotron modes.[12,17] The eigenvalues are well known (see, for example, Ref. 12) and are given by

$$\sigma_l=\pm i\frac{2\pi ecn}{B}[l-1+(r_p/R)^{2l}]. \tag{21}$$

Using a coordinate system centered in the plasma trap, i.e., $x_c=y_c=0$, $\eta=\theta$, the eigenfunction corresponding to the eigenvalue σ_l is given by $e^{\mp il\eta}\equiv e^{\mp il\theta}$. The numerically computed eigenvalues agree with the analytical result given by Eq. (21).

Due to the use of some group theoretic considerations in Sec. IV, let us consider the action of $\mathbf{Z_m}(2\pi/m)$ group on the basis eigenvectors

$$\xi_l^c(\theta)=\cos\ l\theta, \tag{22}$$

$$\xi_l^s(\theta)=\sin\ l\theta, \tag{23}$$

which span the eigenspace for the eigenvalue σ_l for a constant potential $V(\theta)$. These eigenfunctions transform under the action of $\mathbf{Z_m}(2\pi/m)$ as

$$\mathcal{R}(2\pi/m)\xi_l^s(\theta)=\cos\frac{2\pi l}{m}\xi_l^s(\theta)-\sin\frac{2\pi l}{m}\xi_l^c(\theta), \tag{24}$$

$$\mathcal{R}(2\pi/m)\xi_l^c(\theta)=\cos\frac{2\pi l}{m}\xi_l^c(\theta)+\sin\frac{2\pi l}{m}\xi_l^s(\theta), \tag{25}$$

where $\mathcal{R}(2\pi/m)$ denotes a rotation by $2\pi/m$. Two different cases should be distinguished. If $2l/m$ is not an integer then this is an irreducible but not an absolutely irreducible[22] representation of group $\mathbf{Z_m}(2\pi/m)$. In the case where $2l/m$ is an integer, however, the transform reduces to

$$\mathcal{R}(2\pi/m)\xi_l^s(\theta)=(-1)^{2l/m}\xi_l^s(\theta), \tag{26}$$

$$\mathcal{R}(2\pi/m)\xi_l^c(\theta)=(-1)^{2l/m}\xi_l^c(\theta). \tag{27}$$

This representation is a reducible representation of $\mathbf{Z_2}$ when $2l/m$ is an odd integer and of an identity group when $2l/m$ is an even integer.

When a nonconstant wall potential $V(\theta)=-V_0\cos m\theta$ is turned on, the eigenvectors are no longer represented by simple sinusoidal waves due to the coupling between waves with different l. However, the irreducible representations of $\mathbf{Z_m}(2\pi/m)$ associated with the eigenspace for mode l should persist by continuity. We will label the modes by their corresponding values of l in the absence of the external potential. Consider a family of equilibria of a fixed area A_p, and the wall potential $V=V_0F(\theta)$, where $F(\theta)$ is some function of the angle θ and V_0 stands for the strength of the external field. For $V_0=0$ the eigenvalues are purely imaginary and are given by Eq. (21). When the bifurcation parameter rises from zero, the eigenvalues move on the imaginary axis and the spectrum changes. If, at some value of V_0, an eigenvalue with a positive real part appears, then the corresponding equilibrium becomes unstable.

This problem can be considered in a more general context. The dynamical equations for 2D Eulerian fluids are well known to be Hamiltonian.[23] The time evolution of the plasma boundary given by Eq. (16) will be assumed to be Hamiltonian as well. The bifurcation theory of Hamiltonian systems[16,24] predicts that the simplest loss of stability occurs along one of two paths. The first path is through a collision of two eigenvalues at the origin, resulting in the appearance of two eigenvalues with complementary real parts. This path is usually referred to as a steady-state bifurcation. At this bifurcation the system possesses a zero-valued eigenvalue of multiplicity two, and the possibility of crossing with other equilibrium branches must be taken into account. On the second path to instability, two eigenvalues collide at some nonzero frequency and a quadruplet of eigenvalues $\sigma,\sigma^*,-\sigma,-\sigma^*$ with the nonzero real parts emerge. This bifurcation corresponds to a 1–1 resonance, and is called a Hamiltonian–Hopf bifurcation or a Krein collision. Following the terminology used in Ref. 7 the appearance of eigenvalues with real parts as a result of collisions of purely imaginary eigenvalues will be referred to as a splitting of eigenvalues, or simply splitting. As proven in Ref. 7 (and reference therein) splitting is the generic behavior of symmetry-free Hamiltonian systems. In practice, often due to the restrictions imposed on the system by symmetries, eigenvalues do not always follow this generic behavior. Instead of splitting, the eigenvalues sometimes remain on the imaginary axis after collisions and no instability occurs. We will refer to this process as passing.

Let us reconsider the elliptical equilibrium problem with $V=-V_0\cos 2\theta$. We first introduce dimensionless variables

$$A_p^*=\frac{A_p}{\pi R^2},\quad V_0^*=\frac{V_0}{4\pi enR^2},\quad \sigma_l^*=\frac{\sigma_l B}{2\pi ecn}. \tag{28}$$

An example of a highly deformed but stable equilibrium with area $A_p^*=0.3$ at $V_0^*=0.05$ is presented in Fig. 1. As expected, this on-center equilibrium possesses all symmetries of the problem and looks elliptical. The spectrum for a plasma with $A_p^*=0.2$ is obtained numerically for different

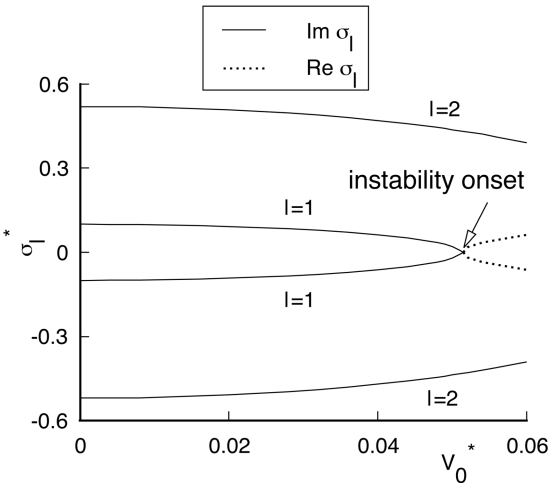

FIG. 4. Spectrum of the elliptical equilibrium.

V_0 as a solution of the eigenvalue problem given by Eq. (20). The results for first two modes are presented in Fig. 4. As the potential V_0 rises from zero, all the eigenvalues begin to move toward the origin on the imaginary axis. The first collision occurs at Im $\sigma_l=0$, and is between the $l=1$ mode and its complex conjugate. As a result, the eigenvalues split and instability occurs.

These numerical results are in agreement with the reduced-Hamiltonian analytical results of Sec. II, but, as the numerical procedure keeps additional harmonic components, it should be more accurate. Numerically, the equilibrium becomes unstable to the $l=1$ diocotron mode. Appropriately, this instability corresponds to the center of charge instability identified in Sec. II. A typical bifurcation diagram with numerical (solid line) and analytical (dashed line) predictions is plotted in Fig. 5. Stable and unstable regions can be seen on the graph. (Note that the stability regions are also limited by the geometrical constraints imposed on the system by the presence of the cylindrical wall.) The analytical model also predicts that another stable equilibrium appears at the bifurcation point. To check this prediction, off-center equilibria were sought with an equilibrium code and their stability was analyzed. No off-center equilibria for potentials below the

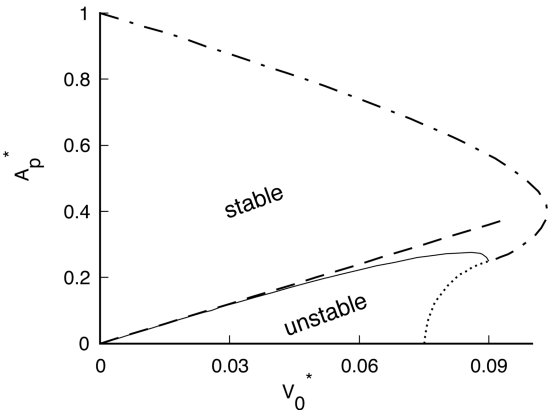

FIG. 5. Stability diagram for the elliptical equilibrium. Threshold of instability from the elliptical plasma model (— — —), from CD (——), geometrical constraint (–·–·–·–), limit of confinement (···).

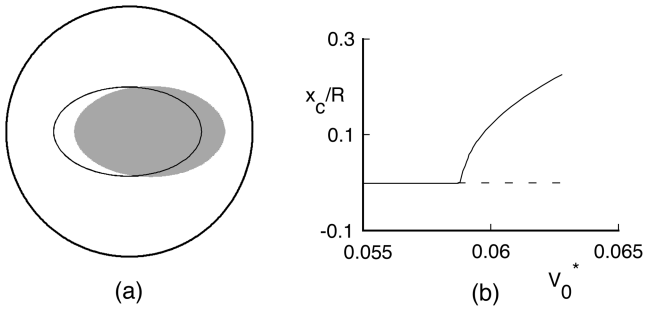

FIG. 6. (a) A stable off-center elliptical equilibrium (shaded). The centered unstable equilibrium (solid line) is plotted for comparison. (b) The position of the center of charge for the center and of center equilibria.

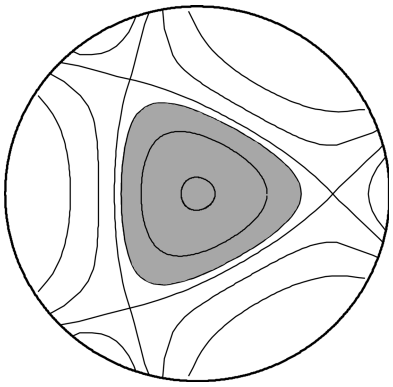

FIG. 7. Triangular on-center equilibrium. The plasma covers the shaded region. The light solid lines are equipotential contours, and the heavy surrounding circle is the trap's cylindrical boundary.

instability threshold were found, but equilibria on the x axis at $\pm x_c$ were obtained above the threshold. An example of an unstable centered and a stable off-center equilibria, with $A_p^*=0.2$ and $V_0^*=0.06$, is presented in Fig. 6. (The unstable on-center equilibrium with ellipticity λ_{02} was also found numerically.)

IV. STABILITY OF SYSTEMS WITH SYMMETRIES

While the detailed physical mechanism responsible for instability is often hard to deduce, some general aspects of the behavior can be predicted based on the symmetries alone. As was mentioned in Sec. III, the generic behavior, i.e., splitting at first collision, can be altered if a symmetry is present in the system. We will merely use the main results derived in Refs. 5 and 7 as they apply to the relation between the type of the symmetry group representation, i.e., absolutely irreducible or nonabsolutely irreducible, and splitting and passing of the eigenvalues at the collision at zero. In a steady-state bifurcation the representation of the symmetry group on the generalized zero eigenspace E_0 (the space spanned by the mode undergoing the collision) is either nonabsolutely irreducible and the eigenvalues pass with nonzero speed, or it is a direct sum of two isomorphic absolutely irreducible subspaces and the eigenvalues split. The eigenvalue motion in a 1–1 resonance is more complicated. Here, the conclusions cannot be made based on the symmetries alone, as energy arguments must be considered as well. General results for the resonant collisions can be found in Ref. 7. Both steady state and resonant collisions will be encountered in the following examples. We will compare the numerical results for steady state bifurcations with the general predictions based on the symmetry of the system. No attempt will be made to compare the resonant collisions with the generic behavior due to the lack of an explicit expression for the symplectic structure of contour dynamics. This is a topic for future work. We first illustrate the use of symmetry arguments by returning to the elliptical equilibrium.

A. Elliptical equilibria revisited

For $V=-V_0\cos 2\theta$ the system has $\mathbf{Z_2}(\pi)$ symmetry with representations given by Eqs. (26) and (27) for any l ($2l/2$ is always an integer). Thus, the generic behavior is the splitting of eigenvalues for any collision at zero. From numerical computation we see that the application of the external potential results in the decrease of the diocotron mode frequencies. The first observed collision is a steady state bifurcation for the mode with the smallest frequency, i.e., for the $l=1$ mode, which results in the instability in accordance with the expected generic behavior. Moreover, a pitchfork bifurcation, which is generic in systems with $\mathbf{Z_2}$ symmetry,[25] is expected. These predictions agree with the results of small plasma analysis and numerical calculations.

We conclude that the numerically observed behavior of the elliptical equilibrium is in agreement with the picture deduced by the symmetry arguments. We expect that all the main features (splitting at the first collision, pitchfork bifurcation for $l=1$ instability) present for the boundary condition $V=-V_0\cos 2\theta$ will remain the same for wall potentials with a twofold axis of symmetry for which the first occurring bifurcation is an $l=1$ steady state collision, but where the potential contains higher order ($\cos 4\theta$, $\cos 8\theta$, etc.) terms. This expectation was verified for the wall potential $V=-V_0$ applied to two 90° patches centered on the x axis.

B. Triangular equilibria

We proceed to a system with a threefold rotation axis. The wall potential is now assumed to be $V=-V_0\cos 3\theta$ with $V_0>0$. The on-center equilibrium appears triangular and possesses all symmetry properties of the system. An example of an equilibrium with $A_p^*=0.2$ and $V_0^*=0.1$ together with its equipotential contours is shown in Fig. 7. Investigation of the spectrum reveals a qualitatively different picture than that for the elliptical plasma. An example of a typical spectrum is presented in Fig. 8 for a plasma with $A_p^*=0.1$. As the bifurcation parameter increases, the eigenvalues move in the direction of Im $\sigma=0$ up until the steady state bifurcation for the $l=1$ mode occurs. However, this collision results in passing and *no* instability takes place. Under the further increase of the bifurcation parameter V_0, the frequency of $l=1$ mode changes sign and moves away from Im $\sigma=0$. All other eigenvalues continue to decrease in absolute value. The resonance between the $l=1$ and $l=2$ modes takes place next, leading to the instability.

This qualitative difference between the elliptical and the triangular cases is anticipated by symmetry arguments. In

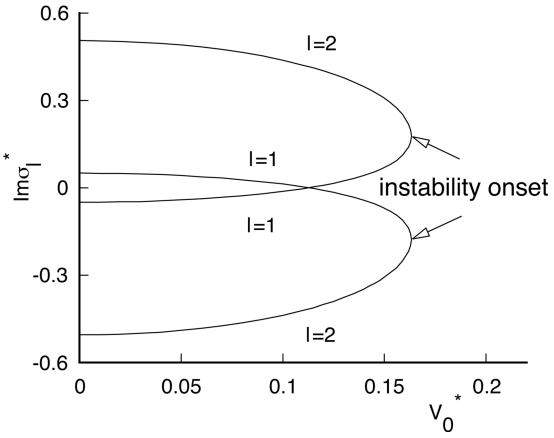

FIG. 8. Spectrum for the triangular on-center equilibrium.

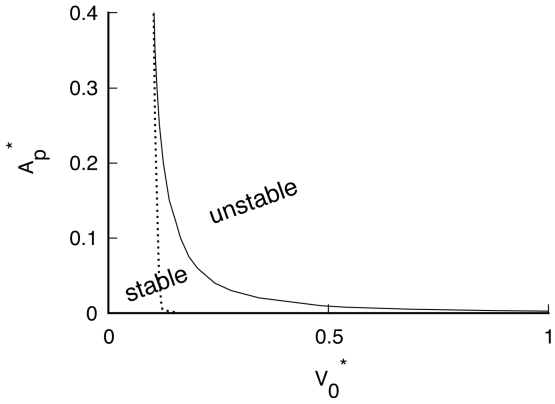

FIG. 10. Stability diagram for the triangular on-center equilibrium. Passing of $l=1$ (···), $l=1,2$ resonant collision with splitting (——).

this case $m=3$ and we have an absolutely irreducible representations (26) and (27) for modes with $l=3,6,9,\ldots,3n,\ldots$ and all other values of l are associated with the nonabsolutely irreducible representations Eqs. (24) and (25). In particular, this is true for $l=1$. Thus, the first observed collision at zero is generically predicted to pass, not split. Moreover, the generic behavior of such systems is crossing with an unstable branch of solutions at bifurcation.[5] The passing bifurcation that takes place is for the $l=1$ mode, which contains the center of charge coordinates. We therefore expect a crossing with an off-center equilibrium branch. This additional equilibrium was subsequently found numerically. Examples of unstable equilibria found before and after the bifurcation point are plotted in Figs. 9(a) and 9(b). The outline of the center stable equilibrium is also plotted (as a solid curve) for a reference. The bifurcation diagram for the center of charge can be seen in Fig. 9(c).

The next bifurcation that takes place is a $l=1,2$ resonance. Numerical results indicate that the $l=1,2$ collision results in an instability. The bifurcation diagram is presented in Fig. 10, where both the steady-state and Krein collision thresholds are plotted.

Note that after the steady-state bifurcation takes place, the frequency of the $l=1$ mode reverses sign. In the language of non-neutral plasmas, this can be phrased as the reversal of the diocotron mode direction of rotation. In other words, if in the absence of the external potential a slightly displaced electron column rotates counterclockwise, after the $l=1$ bifurcation a perturbed equilibrium will rotate clockwise. This prediction was verified numerically. A slightly displaced equilibrium was taken as an initial condition and the time evolution was investigated with a dynamical CD code. The rotation of the center of charge was in the direction opposite to the diocotron rotation when no external potential was present.

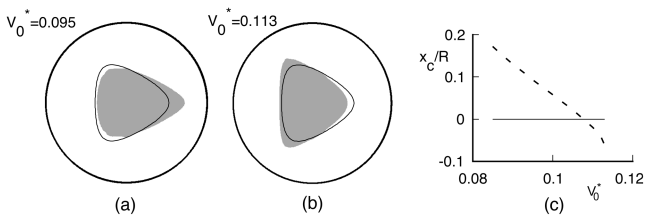

FIG. 9. Triangular unstable (shaded) off-center equilibria: (a) before, (b) after the bifurcation point. The stable centered-equilibrium is indicated by the solid line. (c) The position of the center of charge of different equilibria present in the system.

C. Square equilibria

In the next example a system with a fourfold symmetry axis is considered. The boundary condition is taken as $V=-V_0\cos 4\theta$. The center equilibrium has a square shape. An example of the equilibrium shape corresponding to $V_0^*=0.4$ and $A_p^*=0.1$ is shown in Fig. 11 together with some equipotential contours. The spectrum reveals the following bifurcation picture: first, a steady-state bifurcation occurs for the $l=1$ mode. It results in passing of the eigenvalues. Next, a resonance for the $l=1,2$ quadruplet is observed. These eigenvalues also pass. Finally, a steady-state bifurcation for the $l=2$ mode occurs and splitting results. An example of a spectrum for $A_p^*=0.1$ is presented in Fig. 12.

Again, the motion of eigenvalues at collisions can be qualitatively understood based on the symmetry properties. Now $m=4$, so the absolutely irreducible representations given by Eqs. (26) and (27) take place for any even value of the mode number l and the odd values of l correspond to the

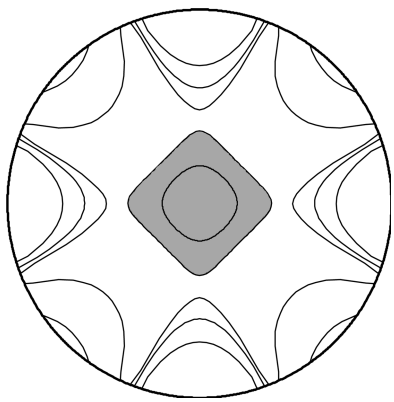

FIG. 11. Stable square on-center equilibrium. The plasma covers the shaded region. The light solid lines are equipotential contours, and the heavy surrounding circle is the trap's cylindrical boundary.

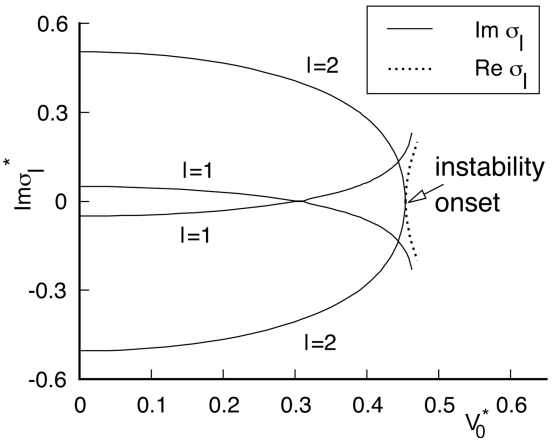

FIG. 12. Spectrum for the square on-center equilibrium.

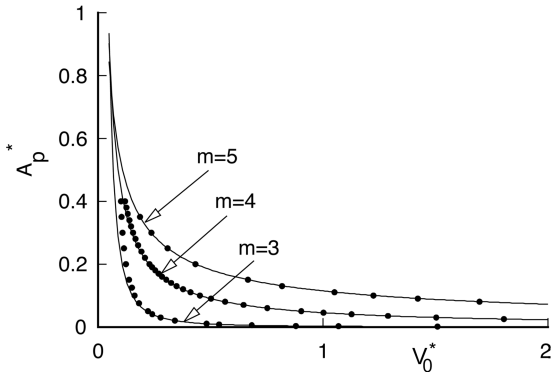

FIG. 14. Numerical (——) and analytical (●) instability thresholds for systems with wall potential $V=-V_0\cos m\theta$ with $m=3,4,5$.

nonabsolutely irreducible case. Therefore, the steady-state collision for $l=1$ mode results in passing, and the collision at zero for $l=2$ should split, in agreement with the numerical results. Also, considering the $l=1$ collision, note that there exist two generic bifurcations for a system with $\mathbf{Z_4}$ symmetry:[5] crossing with two branches (one stable, one unstable), or crossing with one unstable branch. Solutions found numerically correspond to the first case. A stable branch at 45° (four equivalent solutions) and an unstable branch on x axis (four equivalent solutions) are found. The bifurcation is subcritical. An example of these equilibria can be seen in Fig. 13. At the next bifurcation, the collision of $l=1,2$ modes, passing of the eigenvalues is observed. At the next bifurcation, i.e., the $l=2$ collision at zero, the representation for the $l=2$ mode is isomorphic to the representation of $\mathbf{Z_2}$. This situation was already encountered in the case of the $l=1$ bifurcation of the elliptical equilibrium. A pitchfork bifurcation is expected. This unstable branch of solutions was found numerically. The bifurcation is subcritical.

D. Threshold of instability

So far, an analytical result predicting the onset of instability was obtained only for an elliptical equilibrium. We have found a scaling law for the threshold of instability when the wall potential is of the form $V=-V_0\cos m\theta$ with $m>2$. The scaling law follows from the destabilizing effect of the external potential overwhelming the stabilizing plasma potential. Neglecting the contribution of the image, which is important only for elliptical plasma stability, we postulate that instability occurs when the value of the external potential on the plasma surface is of the order of the plasma potential, i.e.,

$$\phi_p(r_p)\sim\phi_{\text{ext}}(r_p). \tag{29}$$

The value of $\phi_{\text{ext}}(r_p)$ can be estimated as

$$\phi_{\text{ext}}(r_p)\sim V_0\left(\frac{A_p}{R^2}\right)^{m/2}. \tag{30}$$

Taking $\phi_p\sim enA_p$, the condition given by Eq. (29) yields

$$\frac{V_0}{enR^2}=C_m\left(\frac{R^2}{A_p}\right)^{m/2-1}, \tag{31}$$

where C_m is a constant, near one, which depends on m. Values for C_m can be determined numerically by finding the instability threshold at one value of R and A_p for each m. The threshold of instability, i.e., the value of the potential V_0 at the onset of instability, was obtained numerically for $m=3$, 4, and 5 by investigating the eigenvalue spectra for different values of the plasma area. Comparison of the numerical results (points) for the threshold of instability with the scaling law given by Eq. (31) ($C_3=1.08$, $C_4=1.78$, and $C_5=2.72$) is presented in Fig. 14. We get good agreement between analytical and numerical results, especially in the region of small area.

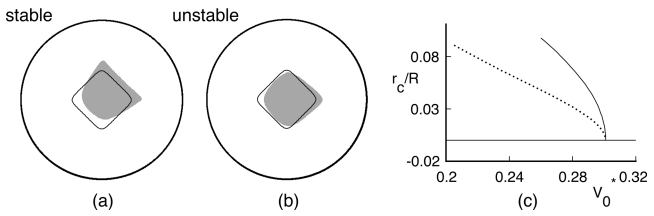

FIG. 13. (a) Stable off-center square equilibrium (shaded). (b) Unstable off-center square equilibrium (shaded). The stable-centered equilibrium is indicated by the solid line. (c) The position of the center of charge of different equilibria present in the system.

V. CIRCULAR OFF-CENTER EQUILIBRIUM

In this last example, we investigate the stability of equilibria in the system with no rotational symmetry. We assume that the wall potential corresponds to a circular equilibrium whose center is located at $(x_c,y_c)=(x_c,0)$. As discussed in the companion paper, this wall potential is simply the free space potential of the cylindrical plasma of area A_p located at $(x_c,0)$, evaluated at the wall. The stability of these circular equilibria can be proved analytically using an extremal energy principle[26] for the case when $x_c<\sqrt{A_p/\pi}$, i.e., the trap origin is inside the plasma. The details of the proof are in Appendix B. To extend the stability analysis to plasmas which do not encompass the origin, we examine the stability numerically and interpret the results in the mode language. The change of the plasma spectrum with the bifurcation parameter x_c for $A_p^*=0.1$ was investigated numerically for the

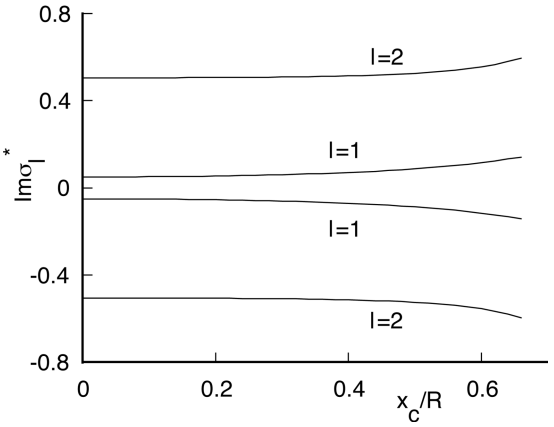

FIG. 15. Spectrum for the off-center circular equilibrium.

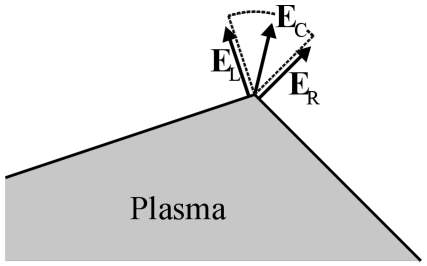

FIG. 16. A blowup of the fields near a sharp corner in a plasma.

first 80 modes. The absolute values of all frequencies were increasing and no resonant collisions occurred in the region of interest $0 \leqslant x_c \leqslant R - \sqrt{A_p/\pi}$. The spectral plot for the first two modes is presented in Fig. 15. As no collisions occur, the equilibrium must be stable.

VI. DISCUSSION

We have considered the linear stability of highly asymmetric plasma equilibria. These equilibria are stable when small wall potentials are applied, but may become unstable when the boundary asymmetries are increased. The elliptical equilibrium, for which an elliptical model can be used, served as a test case to probe different effects that can take place. Transition to instability and crossing with other equilibrium branches were observed. More complicated shapes were analyzed numerically using a technique based on contour dynamics. A modal approach was also used to relate the phenomena occurring at bifurcations to general predictions from the bifurcation theory of Hamiltonian systems.

Several different types of bifurcations were identified. Wall potentials with a dominant $l=1$ harmonic component, which move the equilibrium off the trap center, have a tendency to increase all eigenvalues. Wall potentials with $l \neq 1$ components dominant tend to decrease the mode frequencies, with possible instabilities at the collisions. For the cases investigated here, the first collisions were steady-state bifurcations of the eigenmode with the smallest eigenvalue, namely $l=1$. We showed that the outcomes of the collision are determined by the symmetries present in the system. While the $l=1$ collisions were followed by instability for $V=-V_0 \cos 2\theta$, eigenvalue passing was observed for $V=-V_0 \cos 3\theta$ and $V=-V_0 \cos 4\theta$. Thus, in the presence of certain symmetries, remarkably, some eigenvalue collisions are harmless.

To analyze a general case, we use the following method: from the perturbation analysis, we deduce the initial direction of motion of eigenvalues as the external field is increased. A conclusion on the first collision can often be made. Then, the symmetry analysis of the zero eigenvalue subspace determines whether or not the bifurcation will result in splitting or passing. Furthermore, predictions on the crossing with other equilibrium branches at bifurcation points can be made based on the symmetry.

Unfortunately, we have been unable to find any simple rules for visually determining the stability of a plasma. Generally, the more distorted the plasma is, the more likely it is to be unstable. However, while some relatively circular plasmas may be unstable, other highly distorted plasmas, even plasmas with concave boundaries, may be stable. (The companion paper shows such a concave stable plasma.) Moreover two plasmas which look essentially identical may differ in stability. For example, the two elliptical solutions λ_{01} and λ_{02} can be difficult to distinguish visually, but only the λ_{01} solution is stable. The only completely general visual rule that we have discovered is that any plasma with a sharp corner is unstable. This rule is is easy to establish: Let $\mathbf{E}_L$, $\mathbf{E}_C$, and $\mathbf{E}_R$ be electric fields as shown in Fig. 16. Remembering that the plasma edge is an equipotential, $\mathbf{E}_L$ and $\mathbf{E}_R$ must be at right angles to their respective plasma boundaries. Using the dashed line in the figure as an integration contour, it is clear from Faraday's law that $\mathbf{E}_L$ and $\mathbf{E}_R$ must have the same magnitude. By continuity, $\mathbf{E}_C$ must share this magnitude. But if $\mathbf{E}_c \neq 0$, the region enclosed by the dashed line in not divergence free. As this region can be shrunk to zero, and as there is no surface charge at the plasma boundary, the only way that Faraday and Gauss's laws can be simultaneously satisfied is if $\mathbf{E}_L = \mathbf{E}_C = \mathbf{E}_R = 0$. However, if the electric field at the corner is zero, charge will stagnate in the corner, leading to instability.

To verify that these results are valid when the plasma has a realistically smooth rather than flat-top density profile, we compared the contour dynamics results with a vortex-in-cell (VIC) simulation for elliptical plasmas. Details of the numerical scheme can be found in Ref. 27. We performed a VIC simulation with the density distribution for a plasma in thermal equilibrium[18] (Debye length $\lambda_D \sim 0.2 r_p$). All qualitative features, i.e., existence of a stable elliptical equilibrium on-center, pitchfork bifurcation to a stable equilibrium of center, etc., were verified.

ACKNOWLEDGMENTS

The authors thank B. Boghosian for providing assistance with the vortex-in-cell code, and K. Zukor for her helpful comments. We also thank the referee for many helpful comments on the mathematical aspects of the manuscript. This

work was supported by the Office of Naval Research, the Air Force Office of Scientific Research, and the Department of Energy.

APPENDIX A: LINEAR STABILITY ANALYSIS

In the linear stability analysis, the amplitude of the velocity perturbation $\tilde{\mathbf{v}}$ must be determined as a function of the boundary perturbation $\tilde{\xi}$. Separating the contributions from the plasma, image and external fields, the velocity is

$$\mathbf{v}=\mathbf{v_p}+\mathbf{v_i}+\mathbf{v_{ext}}. \tag{A1}$$

Consider the velocity due to the plasma $\mathbf{v_p}$. From Eq. (11) we obtain

$$\mathbf{v_p}=-\frac{2enc}{B}\oint_C \ln|\mathbf{r}-\mathbf{r}'|d\mathbf{x}'. \tag{A2}$$

Assuming that the boundary perturbation is a normal mode, the resulting velocity perturbation is

$$\tilde{\mathbf{v}}_\mathbf{p}(\eta)=\frac{2enc}{B}\int_0^{2\pi}d\eta'\left[\xi\left(\sin\,\eta\frac{dx_0'}{d\eta'}-\cos\,\eta\frac{dy_0'}{d\eta'}\right)-\xi'\left(\sin\,\eta'\,\frac{dx_0'}{d\eta'}-\cos\,\eta'\,\frac{dy_0'}{d\eta'}\right)\right]\times\frac{(y_0'-y_0,-x_0'+x_0)}{|\mathbf{r_0}-\mathbf{r_0'}|^2}, \tag{A3}$$

where $\mathbf{r_0}=(x_0,y_0)$ corresponds to the radius vector of the equilibrium boundary, and unprimed and primed variables are computed at η, η', respectively. Following Dritschel, the following notations are introduced

$$R(\eta,\eta')=\frac{4\pi enc}{B}\left(\sin\,\eta\frac{dx_0'}{d\eta'}-\cos\,\eta\frac{dy_0'}{d\eta'}\right), \tag{A4}$$

$$Q(\eta)=R(\eta,\eta)=\frac{4\pi enc}{B}\left(\sin\,\eta\frac{dx_0}{d\eta}-\cos\,\eta\frac{dy_0}{d\eta}\right), \tag{A5}$$

$$b^x(\eta,\eta')=\frac{x_0-x_0'}{|\mathbf{r_0}-\mathbf{r_0'}|^2},\quad b^y(\eta,\eta')=\frac{y_0-y_0'}{|\mathbf{r_0}-\mathbf{r_0'}|^2}. \tag{A6}$$

Finally, denoting the integration by $\langle(\ldots)\rangle=1/2\pi\int d\eta'\ldots$, Eq. (A3) can be rewritten as

$$\tilde{v}_p^x=\langle\tilde{\xi}Qb^y\rangle-\tilde{\xi}(\eta)\langle Rb^y\rangle, \tag{A7}$$

$$\tilde{v}_p^y=-\langle\tilde{\xi}Qb^x\rangle+\tilde{\xi}(\eta)\langle Rb^x\rangle. \tag{A8}$$

The plasma velocity perturbation is now given as a linear functional of $\tilde{\xi}$. Turning to the image velocity $\mathbf{v_i}$, the image potential is a solution of Laplace's equation subject to the boundary condition $\phi_i(R,\theta)=-\phi_p(R,\theta)$. Calculating $\mathbf{v_i}=-c\nabla\phi_i\times\hat{z}/B$ in polar coordinates, and expressing it through the boundary condition for velocity, we obtain

$$v_i^x=2\sum_{l=1}^{\infty}\left(\frac{r}{R}\right)^{l-1}[\mathrm{Re}\;V_l^r\cos(l-1)\theta+\mathrm{Im}\;V_l^r\sin(l-1)\theta], \tag{A9}$$

$$v_i^y=2\sum_{l=1}^{\infty}\left(\frac{r}{R}\right)^{l-1}[-\mathrm{Re}\;V_l^r\sin(l-1)\theta+\mathrm{Im}\;V_l^r\cos(l-1)\theta], \tag{A10}$$

where V_l^r stands for the Fourier transform of the radial component of the image velocity at the confining wall

$$V_l^r=-\frac{1}{2\pi}\int_0^{2\pi}d\theta v_p^r(R,\theta)e^{il\theta}. \tag{A11}$$

We can calculate the r component of the plasma velocity at the confining wall, $v_p^r(R,\theta)$, explicitly using Eq. (A2). Examining the amplitude of the perturbation to linear order, two contributions are manifest. The contribution due to the change of the plasma velocity, i.e., the boundary condition for the image, can be calculated analogously to Eq. (A3). The change in the velocity due to the change of the boundary position is also important. Combining these two effects, the amplitude of the image velocity perturbation becomes

$$\tilde{v}_i^x=\sum_{l=1}^{\infty}[\langle\tilde{\xi}QZ_l\rangle A_l(\eta)+\langle\tilde{\xi}QW_l\rangle B_l(\eta)]+\tilde{\xi}T_x(\eta), \tag{A12}$$

$$\tilde{v}_i^y=\sum_{l=1}^{\infty}[\langle\tilde{\xi}QW_l\rangle A_l(\eta)-\langle\tilde{\xi}QZ_l\rangle B_l(\eta)]+\tilde{\xi}T_y(\eta), \tag{A13}$$

where

$$A_l(\eta)=2\left(\frac{r_0}{R}\right)^{l-1}\cos(l-1)\theta_0,$$

$$B_l(\eta)=2\left(\frac{r_0}{R}\right)^{l-1}\sin(l-1)\theta_0,$$

$$Z_l(\eta)=\frac{1}{2\pi}\int_0^{2\pi}d\theta\frac{y_0\cos\,\theta-x_0\sin\,\theta}{|\mathbf{r_0}-\mathbf{R}|^2}\cos l\theta,$$

$$W_l(\eta)=\frac{1}{2\pi}\int_0^{2\pi}d\theta\frac{y_0\cos\,\theta-x_0\sin\,\theta}{|\mathbf{r_0}-\mathbf{R}|^2}\sin l\theta,$$

$$T_x(\eta)=2\sum_{l=1}^{\infty}\left(\frac{r_0}{R}\right)^{l-2}(l-1)[\mathrm{Re}\;V_{l0}^r\cos(\eta+(l-2)\theta_0)+\mathrm{Im}\;V_{l0}^r\sin(\eta+(l-2)\theta_0)],$$

$$T_y(\eta)=2\sum_{l=1}^{\infty}\left(\frac{r_0}{R}\right)^{l-2}(l-1)[-\mathrm{Re}\;V_{l0}^r\sin(\eta(l-2)\theta_0)+\mathrm{Im}\;V_{l0}^r\cos(\eta+(l-2)\theta_0)], \tag{A14}$$

with V_{l0}^r calculating using the equilibrium shape. Similarly, the amplitude of the external velocity perturbation is

$$\tilde{v}_{\mathrm{ext}}^x=\tilde{\xi}S_x(\eta),\quad \tilde{v}_{\mathrm{ext}}^y=\tilde{\xi}S_y(\eta), \tag{A15}$$

where

$$S_x(\eta)=2\sum_{l=1}^{\infty}\left(\frac{r_0}{R}\right)^{l-2}l(l-1)[\mathrm{Re}\;V_l\sin(\eta+(l-2)\theta_0)-\mathrm{Im}\;V_l\cos(\eta+(l-2)\theta_0)],$$

$$S_y(\eta)=2\sum_{l=1}^{\infty}\left(\frac{r_0}{R}\right)^{l-2} l(l-1)[\mathrm{Re}\ V_l\cos(\eta+(l-2)\theta_0) + \mathrm{Im}\ V_l\sin(\eta+(l-2)\theta_0)], \tag{A16}$$

and where V_l is the Fourier transform of the boundary condition for the potential on the confining wall

$$V_l=\frac{1}{2\pi}\int_0^{2\pi} d\theta V(\theta)e^{il\theta}. \tag{A17}$$

Combining Eqs. (A7), (A8), (A12), (A13), and (A15) the total velocity perturbation is

$$\tilde{\mathbf{v}}=\tilde{\mathbf{v}}_\mathbf{p}+\tilde{\mathbf{v}}_\mathbf{i}+\tilde{\mathbf{v}}_\mathbf{ext}. \tag{A18}$$

Expanding Eq. (18), the boundary disturbance is

$$\tilde{\xi}(\eta)=\xi_0(\eta)\lim_{N_l\to\infty}\sum_{l=1}^{N_l} C_l f_l(\eta). \tag{A19}$$

In practice, only a finite number of basis functions are kept in this expansion. Upon substitution into the equation of motion given by Eq. (17):

$$\varepsilon=\sigma\tilde{\xi}+v_{\eta 0}\frac{d}{d\eta}\frac{\tilde{\xi}}{\xi_0}+\frac{\tilde{v}_\eta}{\xi_0}\frac{d\xi_0}{d\eta}-\frac{1}{v_{\eta 0}}(\tilde{v}_x v_{y0}-\tilde{v}_y v_{x0})\neq 0. \tag{A20}$$

Following the Galerkin method, we demand that the error ε is orthogonal to each of the basis functions f_l, i.e.,

$$\int_0^{2\pi} d\eta\varepsilon f_l=0,\quad l=1,2\ldots N_l. \tag{A21}$$

This requirement results in N_l equations for N_l unknown coefficients C_l, which can be written in matrix form as

$$\sigma C_m=\sum_{l=1}^{N_l} G_{ml}C_l, \tag{A22}$$

where

$$G_{ml}=G^1_{ml}+G^2_{ml}+G^3_{ml}+G^4_{ml}+G^5_{ml},$$

$$G^1_{ml}=-2\pi\left\langle\frac{v_{\eta 0}}{\xi_0}f_m\frac{df_l}{d\eta}\right\rangle,$$

$$G^2_{ml}=2\pi\left\langle\frac{v_{y0}}{v_{\eta 0}\xi_0}f_m\langle f_l\xi_0 Rb^y\rangle\right\rangle + 2\pi\left\langle\frac{v_{x0}}{v_{\eta 0}\xi_0}f_m\langle f_l\xi_0 Rb^x\rangle\right\rangle,$$

$$G^3_{ml}=-2\pi\left\langle\frac{v_{y0}}{v_{\eta 0}}f_m f_l\langle Qb^y\rangle\right\rangle-2\pi\left\langle\frac{v_{x0}}{v_{\eta 0}}f_m f_l\langle Qb^x\rangle\right\rangle,$$

$$G^4_{ml}=2\pi\left\langle\frac{v_{y0}}{v_{\eta 0}}f_m f_l(S_x+T_x)\right\rangle - 2\pi\left\langle\frac{v_{x0}}{v_{\eta 0}}f_m f_l(S_y+T_y)\right\rangle,$$

$$G^5_{ml}=2\pi\left\langle\frac{v_{y0}}{v_{\eta 0}\xi_0}f_m D_l\right\rangle-2\pi\left\langle\frac{v_{x0}}{v_{\eta 0}\xi_0}f_m F_l\right\rangle,$$

$$D_l=2\sum_{k=1}^{N_l/2} r_0^{k-1}[\mathrm{Re}\ N_{lk}\cos(k-1)\theta_0 + \mathrm{Im}\ N_{lk}\sin(k-1)\theta_0],$$

$$F_l=-2\sum_{k=1}^{N_l/2} r_0^{k-1}[\mathrm{Re}\ N_{lk}\sin(k-1)\theta_0 - \mathrm{Im}\ N_{lk}\cos(k-1)\theta_0],$$

$$N_{lk}=\int_0^{2\pi} d\theta e^{ik\theta}\left\langle\frac{\xi_0 f_l Q}{|\mathbf{r_0}-\mathbf{R}(\theta)|^2}(y_0\cos\theta-x_0\sin\theta)\right\rangle. \tag{A23}$$

APPENDIX B: STABILITY OF CIRCULAR OFF-AXIS EQUILIBRIA

The stability for circular equilibria can be readily proved using O'Neil and Smith's energy principle.[26] Since we assume that the plasma motion is solely due to $\mathbf{E}\times\mathbf{B}$ drifts, the electrostatic energy of the plasma is conserved if the wall voltages are time independent. If the electrostatic energy of a given plasma is extremal, there are no nearby accessible states because such states would have different energy. Consequently the plasma must be stable. Using this principle, Chu *et al.* proved that slightly deformed plasmas are energy maxima and, consequently, are stable. Here we prove that any circular, off-axis plasma which encompasses the origin, is stable.

Given any circular plasma of radius r_p, all nearby shapes can be represented by the series,

$$R_p^2(\theta)=r_p^2(\theta)+\sum_{m=1}^{\infty}(F_m\sin m\theta+G_m\cos m\theta), \tag{B1}$$

where (F_m,G_m) are small. As is required for $\mathbf{E}\times\mathbf{B}$ drifts, this series conserves the area of the plasma. To first order, the old boundary is perturbed a distance

$$\Delta R_p(\theta)=\frac{1}{2r_p}\sum_{m=1}^{\infty}(F_m\sin m\theta+G_m\cos m\theta). \tag{B2}$$

Think of this new boundary as having been generated by the superposition of appropriate amounts of positive and negative charge. Charge of density $n_+=n$ extends the boundary outward, while charge of density $n_-=-n$ pushes the boundary inward. The energy necessary to create this perturbation can be split into two parts: the self-assembly energy U_A necessary to create the surface charge $\sigma(\theta)=ne\Delta R_p(\theta)$ on the original boundary r_p, and the distribution energy U_D necessary to distribute this charge off the original boundary. Since the original boundary is an equipotential, no energy is necessary to distribute the surface charge along the boundary itself.

The distribution energy equals $\int d\theta r_p E_r\sigma(\theta)\Delta R_p(\theta)/2$ where E_r is the electric field created by the bulk plasma. Evaluating yields

$$U_\mathrm{D}=-\frac{(\pi en)^2}{4}\sum_{m=1}^{\infty}(F_m^2+G_m^2), \tag{B3}$$

and is negative definite. The self-assembly energy equals $\int d\theta r_p \sigma(\theta)\Psi_s(\theta)/2$, where Ψ_s is the potential created by the surface charge itself. Since the boundary is circular, this potential is readily evaluated. Ignoring the surface charge induced image charges, the self-assembly energy equals

$$U_{A0}=\frac{(\pi en)^2}{4}\sum_{m=1}^{\infty}\frac{F_m^2+G_m^2}{m}, \tag{B4}$$

and is positive definite. The image of the surface charge at some angle θ_0 is at R^2/r_p. Using a standard expansion,[28] the image charge field is

$$\Psi_I(\theta)=-2\int_0^{2\pi}d\theta_0 r_p\sigma(\theta_0)\left\{-\ln\left[\frac{R^2}{r_p}\right]+\sum_{p=1}^{\infty}\frac{1}{p}\left[\frac{r_p}{R}\right]^{2p}(\cos p\theta_0\cos p\theta+\sin p\theta_0\sin p\theta)\right\}. \tag{B5}$$

This expansion is only valid for $r_p<R$, and limits this proof to plasmas which encompass the origin. The image field energy is $\int d\theta r_p\sigma(\theta)\Psi_I(\theta)/2$. Substituting for σ, and rearranging gives terms of the form

$$-(en)^2\sum_{p=1}^{\infty}\frac{1}{pR^{2p}}\int_0^{2\pi}d\theta r_p^{p+1}\Delta R_p(\theta)\begin{Bmatrix}\cos p\theta\\ \sin p\theta\\ r_p^{-p}\end{Bmatrix}\times\int_0^{2\pi}d\theta_0 r_p^{p+1}\Delta R_p(\theta)\begin{Bmatrix}\cos p\theta_0\\ \sin p\theta_0\\ \ln[R^2/r_p]\end{Bmatrix}. \tag{B6}$$

The first two rows of this expression gives terms which are the square of a single integral, and the last row integrates to zero. Thus the self-assembly energy from the image charge equals

$$U_{AI}=-\frac{(en)^2}{2}\sum_{p=1}^{\infty}\frac{1}{pR^p}\left\{\left[\int_0^{2\pi}d\theta\sum_{m=1}^{\infty}(F_m\sin m\theta+G_m\cos m\theta)r_p^p\cos p\theta\right]^2+\left[\int_0^{2\pi}d\theta\sum_{m=1}^{\infty}(F_m\sin m\theta+G_m\cos m\theta)r_p^p\sin p\theta\right]^2\right\}, \tag{B7}$$

and is negative definite. The total energy is the sum of these three contributions:

$$U_{tot}=U_D+U_{A0}+U_{AI}=U_{AI}-\frac{(\pi en)^2}{4}\sum_{m=1}^{\infty}(F_m^2+G_m^2)\left(1-\frac{1}{m}\right), \tag{B8}$$

is negative definite for any nonzero perturbation. Therefore any circular plasma that encompasses the origin is stable.

[1] J. Notte, A. J. Peurrung, J. Fajans, R. Chu, and J. Wurtele, Phys. Rev. Lett. **69**, 3056 (1992).
[2] J. A. Notte, Ph.D. thesis, University of California, Berkeley, 1993.
[3] J. Notte and J. Fajans, Phys. Plasmas **1**, 1123 (1994).
[4] J. Fajans, E. Y. Backhaus, and J. E. McCarthy, Phys. Plasmas **6**, 12 (1999); see, also, J. E. McCarthy, E. Y. Backhaus, and J. Fajans, J. Math. Phys. **39**, 6720 (1998).
[5] M. Golubitsky and I. Stewart, Physica D **24**, 391 (1987).
[6] M. Golubitsky, I. Stewart, and D. Schaeffer, *Singularities and Groups in Bifurcation Theory*, Applied Mathematical Sciences Vol. 69 (Springer, New York, 1988).
[7] M. Dellnitz, I. Melbourn, and J. Marsden, Nonlinearity **5**, 979 (1992).
[8] J. H. Malmberg, C. F. Driscoll, B. Beck, D. L. Eggleston, J. Fajans, K. Fine, X. P. Huang, and A. W. Hyatt, in *Non-Neutral Plasma Physics*, edited by C. W. Roberson and C. F. Driscoll, AIP Conf. Proc. No. 175 (American Institute of Physics, New York, 1988) p. 28.
[9] *Non-Neutral Plasma Physics*, edited by C. W. Roberson and C. F. Driscoll, AIP Conf. Proc. No. 175 (American Institute of Physics, New York, 1988).
[10] *Non-Neutral Plasma Physics II*, edited by J. Fajans and D. H. E. Dubin AIP Conf. Proc. No. 331 (American Institute of Physics, New York, 1995).
[11] R. H. Levy, Phys. Fluids **8**, 1288 (1965).
[12] R. C. Davidson, *Physics of Non-Neutral Plasmas* (Addison-Wesley, Redwood City, CA, 1990).
[13] R. Chu, J. S. Wurtele, J. Notte, A. J. Peurrung, and J. Fajans, Phys. Fluids B **5**, 2378 (1993).
[14] N. J. Zabusky, M. H. Hughes, and K. V. Roberts, J. Comput. Phys. **30**, 96 (1979).
[15] E. Y. Backhaus, J. Fajans, and J. S. Wurtele, J. Comput. Phys. **145**, 462 (1998).
[16] R. Abraham and J. Marsden, *Foundation of Mechanics*, 2nd ed. (Addison Wesley, New York, 1978).
[17] W. D. White, J. H. Malmberg, and C. F. Driscoll, Phys. Rev. Lett. **49**, 1822 (1982).
[18] S. A. Prasad and T. M. O'Neil, Phys. Fluids **22**, 278 (1979).
[19] G. S. Deem and N. J. Zabusky, Phys. Rev. Lett. **40**, 859 (1978).
[20] D. G. Dritschel, Comput. Phys. Rep. **10**, 77 (1989).
[21] D. G. Dritschel, J. Fluid Mech. **157**, 95 (1985).
[22] A representation of a group Γ on the vector space V is absolutely irreducible if the only linear mappings $V\rightarrow V$ that commute with Γ are scalar multiples of identity. More details on this and other group theoretical definitions can be found in Chap. XII of Ref. 6.
[23] P. Morrison, Rev. Mod. Phys. **70**, 467 (1998).
[24] R. S. MacKay, in *Nonlinear Phenomena and Chaos*, edited by S. Sarkar (Hilger, Boston, 1986), p. 254.
[25] J. Guckenheimer and P. Holmes, *Nonlinear Oscillations, Dynamical Systems, and Bifurcations of Vector Fields*, Applied Mathematical Sciences Vol. 42 (Springer, New York, 1986).
[26] T. M. O'Neil and R. A. Smith, Phys. Fluids B **4**, 2720 (1992).
[27] R. Chu, Ph.D. thesis, Massachusetts Institute of Technology, 1993.
[28] W. R. Smythe, *Static and Dynamic Electricity* (McGraw-Hill, New York, 1950).